ON THE INFLUENCE OF COUPLING AMC RESONANCES FOR RCS REDUCTION IN THE SHF BAND

M. E. de Cos[*], Y. Álvarez, and F. Las-Heras

Área de Teoría de la Señal y Comunicaciones, Universidad de Oviedo, Edif. Polivalente, Mod. 8, Campus Universitario de Gijón, Gijón (Asturias) E-33203, Spain

Abstract—A novel approach to Radar Cross-Section reduction using a thin Artificial Magnetic Conductor (AMC) structure is presented. The novel AMC structure combines two unit-cell metallization sizes and so it presents two resonant frequencies. RCS reduction is based on destructive interference of two partial reflections. Taking as starting point a previous work showing significant RCS reduction based on the combination of two AMC surfaces with overlapped AMC operation bandwidths (so that they have similar reflection coefficient amplitude) without a 180°-phaseshift, the key point of this contribution is to analyze the influence of the degree of the aforementioned overlapping on RCS reduction and to show that this achievement is based on coupling phenomena. A comparison of the achieved RCS reduction when combining two AMCs whose AMC operation bandwidth overlaps, two AMCs with non-overlapped AMC operation bandwidths, and PEC-AMC is presented. Prototypes of these three combinations have been manufactured (having them the same size) and their RCS has been measured in an anechoic chamber.

1. INTRODUCTION

For many years, Radar Cross Section (RCS) [1–9] reduction has been a field of interest for different applications where the goal is the reduction of the scattered electromagnetic field when illuminating the object-of-interest by an incident wave [10–28]. Depending on the emitting and receiving device, RCS can be monostatic (the transmitter and the

receiver are placed at the same position) or bistatic (they do not share the same position). Different solutions have been proposed for RCS reduction: the use of Radiation Absorbing Material (RAM) [11, 12], object shaping [13], object coating [14–17], and in the last years, object cloaking [18, 19].

A combination of RAM and coating techniques is the so-called Salisbury screen, a resistive dielectric sheet placed $\lambda/4$ above a perfect electric conductor (PEC) surface [20–22]. The use of artificial magnetic surfaces, whose reflection coefficient is $\rho = +1$, was discussed by Fante and McCormack in [21], highlighting the fact of thickness reduction with respect to the Salisbury screen. [23–28] describes the use of metamaterials for RCS reduction.

Combination of PEC and AMC surfaces in a chessboard-like structure has been proposed by Zhang et al. [29] and Paquay et al. [30], as well as tested in [37]. The idea is to obtain two reflected waves with a 180° phaseshift between them (thus cancelling each other), as the reflection coefficient of PEC surfaces is $\rho = -1$, whereas artificial magnetic conductors (AMCs) present $\rho = +1$. In the same way, and using the property that AMCs behave as PEC outside the AMC operation bandwidth, a combination of two AMC which different resonant frequencies is proposed in [32, 33] (in a chessboard-like fashion) and [29] (fan-type structure).

The combined structures must exhibit a 180°-phaseshift together with the same reflection coefficient amplitude, $|\rho|_{\text{PEC}} = |\rho|_{\text{AMC}}$, in order to achieve a full destructive interference. However, AMC surfaces can present $|\rho|_{\text{AMC}} < 1$, so the reflected waves on the combined surface do not completely cancel each other, as concluded in [38]. In addition, it is possible to obtain a large RCS reduction even if a 180°-phaseshift is not achieved provided that the combined surfaces have the same reflection coefficient amplitude. These conclusions are supported by Fig. 1, where the amplitude of the reflected wave as a function of $|\rho|_{\text{AMC}}$ and the phaseshift $< \rho >_{\text{PEC}} - < \rho >_{\text{AMC}}$ is depicted.

Starting from the work described in [38], the aim of this contribution is to study the effects on RCS reduction when the AMC operation bandwidth overlaps or not. It is believed that coupling resonances would yield to larger RCS reduction. To support this, two AMC prototypes, one with overlapped AMC operation bandwidth (the same as in [38]) and other with separated bands are manufactured and measured. In addition, an analysis based on the Array Factor Theory is introduced, to see if this analysis can predict (or not) RCS reduction in the presence of coupling phenomena.
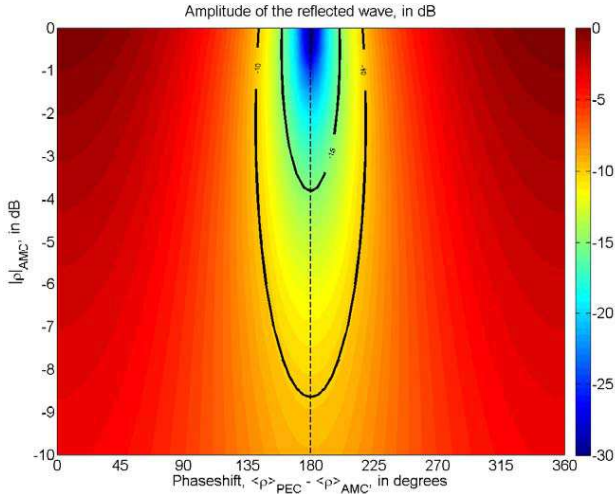
Figure 1. Combined PEC-AMC reflected wave amplitude as a function of $|\rho|_{\mathrm{AMC}}$ and the phaseshift $< \rho >_{\mathrm{PEC}} - < \rho >_{\mathrm{AMC}}$ ($|\rho|_{\mathrm{PEC}} = 1$).

2. AMC DESIGN

The proposed AMC surface (structure) is based on the unit cell described in [34, 35], designed to work in the 5.8 GHz SHF band. The main advantages of this structure are that neither via holes nor multilayer substrates are required, simplifying its practical implementation and its integration with objects (planar microwave devices) as well as reducing its cost. Other advantages that can be highlighted are low dielectric losses, planar feature and low profile ($\lambda/67$).

The designed unit cell geometry is shown in [38]. A dielectric substrate, Arlon 25N, with relative dielectric permittivity, $\varepsilon_r = 3.28$, loss tangent less than 0.0025 and a thickness of $h = 0.762$ mm (30 mils), is used. Unit cell dimensions are $W \times W = 9.6$ mm $\times$ 9.6 mm and its geometry exhibits four symmetry planes. The metallization thickness is 18 µm. This first prototype (denoted as AMC #1) operates at 5.87 GHz and the AMC operation bandwidth is approximately 150 MHz (2.5%) [35].

The metallization of this unit cell (AMC #1) has been scaled (by reducing its size in a 1% factor) in order to obtain another unit cell, AMC #2, with different (higher) resonance frequency (5.96 GHz) [38]. The AMC operation bandwidth of both resulting combinations (AMC

#1 and AMC #2) overlaps since the two unit cells' metallization size
is very similar (see Fig. 2). The reflected waves in these two AMC
surfaces shall not completely cancel each other because the phase
difference between AMC #1 and AMC #2 is less than 180°.

    Next step is the design of another AMC (AMC #3) so that its
phase difference with respect to AMC #1 is 180° in the frequency
band between the resonance frequencies of AMC #1 and AMC #3.
The metallization of the AMC #3 is the same as AMC #1 but reduced
by a 3% factor, obtaining a resonance frequency at 6.30 GHz. From
the results shown in Fig. 2, it is possible to appreciate that the phase
difference between AMC #1 and AMC #3 is close to 180° at the
resonance frequencies. Also, their AMC frequency bands are not
overlapping, as in the case of AMC #1 and AMC #2 designs.
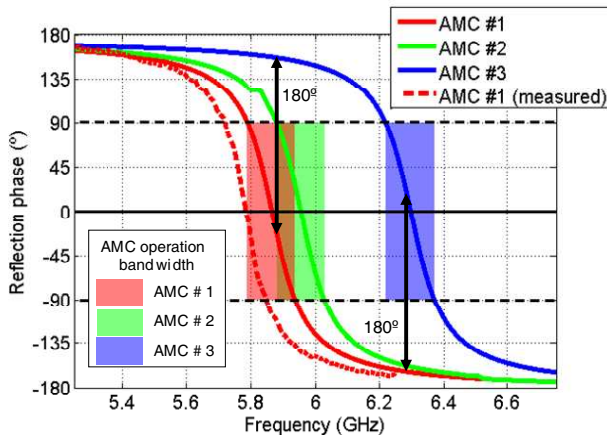
Figure 2. Simulated AMC reflection phase vs. frequency, and
measured AMC reflection phase for AMC #1. Overlapped bands
of AMC #1 and AMC #2 and non-overlapped bands of AMC #1
and AMC #3. Phase difference between #1 and #3 is 180° at two
frequencies.
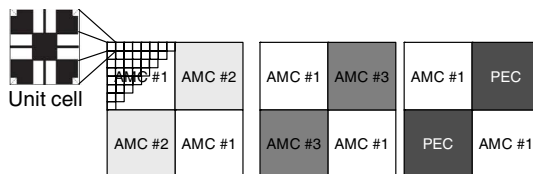
Figure 3. AMCs combinations in different 2 × 2 chessboard-like
geometries: AMC #1,2; AMC #1,3; AMC #1, PEC.

Unit cells are combined in groups of 8×8 cells, being again combined in a 2×2 chessboard-like geometry (see Fig. 3), denoted as AMC #1,2 and AMC #1,3. A third design is obtained by combining the AMC #1 and a PEC surface [37, 38] (see Fig. 3), so that a 180° phaseshift is achieved when the AMC #1 reflection phase is zero (at around 5.87 GHz).

3. RESULTS

Three planar AMC prototypes with 16×16 cells have been manufactured using laser micromachining: the first one is a combination of prototypes AMC #1 and AMC #2 (AMC #1,2; see [38]), the second one combines AMC #1 and AMC #3 (AMC #1,3), and the last one is a combination of AMC #1 and PEC surface (AMC #1-PEC; see [37, 38]).

Typically, a 1.5% deviation (frequency shift) between simulation and measurement values is observed. As described in [35], a manufactured prototype of AMC #1 has the resonance at the frequency of $f = 5.78$ GHz, whereas simulation renders a resonance frequency of 5.87 GHz (see Fig. 2). This can be attributable to the manufacturing process as justified in [36] and also to the variation of relative dielectric permittivity (ε_r) with respect to its nominal value used in the simulations.

3.1. Measurement Setup in Anechoic Chamber

An RCS measurement setup has been arranged based on the spherical range in anechoic chamber of the "AntEM–Lab-Universidad de Oviedo" in order to test the manufactured AMC prototypes, as shown in Fig. 4. A complete description of the measurement setup can be found in [37, 38].

A roll-over-azimuth positioner, covered by flat laminate RAM (in order to minimize reflections due to the metallic positioner structure) is used to place the object-under-test. Two horn antenna probes working in the 5–7 GHz band have been chosen as Tx and Rx antennas. The separation between each probe and the object-under-test is $R_{\mathrm{meas}} = 3$ m ensuring far field conditions.

The manufactured AMC prototypes are tested for different incidence (θ_{inc}) and scattering (θ_{scatt}) angles, which depend not only on the position of the Tx-Rx horn antennas but also on the azimuth angle (θ_{az}) of the object-under-test positioner [37, 38]. The object-under-test can be also rotated in roll (φ-angle), so the RCS response for different field polarization angles can be evaluated (see Fig. 4).
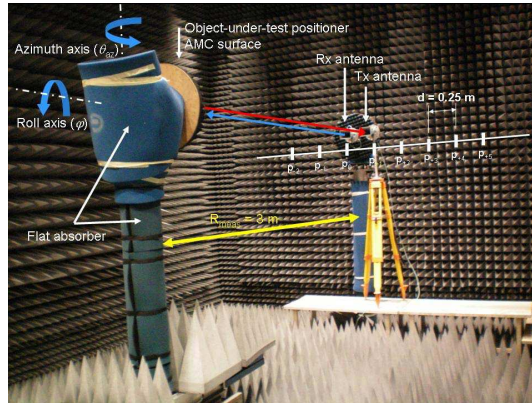
Figure 4. Photo of the RCS measurement setup at the spherical range in anechoic chamber.

3.2. Characterization Regarding Quasi-normal Incidence

The AMC frequency response is obtained under quasi-normal incidence (or quasi-monostatic RCS measurement, as $\theta_{\text{inc}} = \theta_{\text{scatt}} = 2.3°$ [37, 38]). Fig. 5 represents the reflection coefficient amplitude of the three manufactured prototypes (AMC #1,2 [38]; AMC #1,3; and AMC #1-PEC) and the response of the AMC #1 prototype presented in [35] compared to the response of a metallic plate (PEC). All the manufactured prototypes (including the PEC) have the same size ($15.36 \times 15.36 \, \text{cm}$). In order to compare the three prototypes, their reflection coefficient amplitude plotted in Fig. 5 is normalized with respect to the maximum of a same-sized PEC response.

Measurements plotted in Fig. 5 show that the AMC #1 reflection coefficient amplitude ($|\rho|_{\text{AMC}\#1}$) is approximately 7 dB lower than the PEC ($|\rho|_{\text{PEC}}$) at $f = 5.78 \, \text{GHz}$ (which is AMC #1 resonance frequency [35]).

The results presented in Fig. 5 showing that AMC #1-PEC prototype is not able to reduce the RCS in more than 15 dB agree with Fig. 1 which predicts that combination of two waves reflected on PEC and AMC #1 surfaces should not cancel completely.

In the case of the AMC #1,3 prototype, there are two frequency bands centered in $f_1 = 5.77 \, \text{GHz}$ and $f_2 = 6.15 \, \text{GHz}$, where the phaseshift between AMC #1 and AMC #3 is 180° (see Fig. 2). Again, $|\rho|_{\text{AMC}\#1}$ is different from $|\rho|_{\text{AMC}\#3}$ at these frequencies due to its different behavior (at f_1, AMC #3 presents PEC characteristics), so full destructive interference is not achieved.
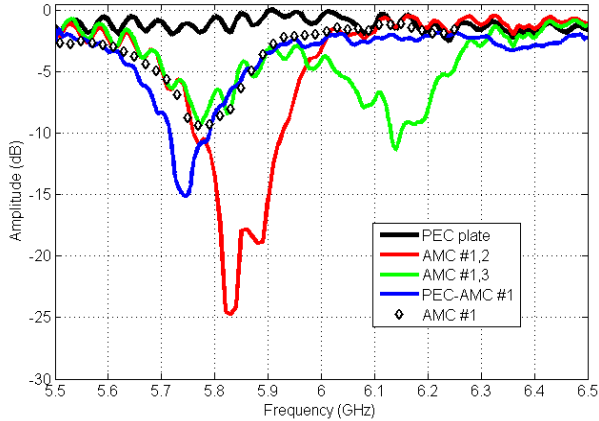
Figure 5. Measured scattered field amplitude for different objectsunder-test: prototypes AMC #1,2, AMC #1,3, AMC #1-PEC, only AMC #1, and the metallic plate ("PEC"). Quasi-normal incidence ($\theta_{\text{inc}} = \theta_{\text{scatt}} = 2.3°$, $\varphi = 0°$).

Finally, the most significant RCS reduction (more than 15 dB in a bandwidth of 95 MHz (1.6% relative to the center frequency) is achieved for AMC #1,2 prototype exhibiting less than 180° phaseshift (160° at most) which yields a non-complete destructive interference. However, due to the overlapped AMC operation bandwidth of the combined AMCs (AMC #1 and AMC #2), both $|\rho|_{\text{AMC}\#1}$ and $|\rho|_{\text{AMC}\#2}$ are similar, which contribute to mutual cancellation of the reflected waves even without a 180°-phaseshift.

3.3. Comparison with Array Factor Theory

As stated before, one of the goals of this paper is to test if RCS reduction can be predicted or not using Array Factor Theory when the AMC operation bandwidths of combined AMCs overlap. It has been previously shown that if they not overlap, Array Factor Theory can be used to predict the expected RCS reduction as presented in [30]. This section describes a comparison between the predicted RCS pattern using Array Factor Theory (for a 2×2 chessboard-like structure) and the measured RCS patterns.

For the theoretical study, the measured reflection coefficient of each single prototype (AMC #1, AMC #2, AMC #3, PEC) is considered at the frequency at which each prototype combination (AMC #1- PEC, AMC #1,2 AMC #1,3) is measured. This reflection coefficient corresponds to the lowest RCS value achieved by each prototype (see Fig. 5), as summarized in Table 1.

Table 1. Reflection coefficient of the combined prototypes at the frequency where maximum RCS reduction is achieved.

Prototype AMC #1-PEC RCS reduction: 15 dB @ $f = 5.74$ GHz	Surface 1: AMC #1	$\|\rho\|_{\text{AMC \#1}} = -6.4\,\text{dB}$ $<\rho>_{\text{AMC \#1}} = 40°$
	Surface 2: PEC	$\|\rho\|_{\text{PEC}} = 0\,\text{dB}$ $<\rho>_{\text{PEC}} = 180°$
	Reflection coefficient difference	$\|\rho\|_{\text{AMC \#1}} - \|\rho\|_{\text{PEC}} = 6.4\,\text{dB}$ $\|\rho\|_{\text{AMC \#1}}$ $- <\rho>_{\text{PEC}} = 140°$
Prototype AMC #1,2 RCS reduction: 25 dB @ $f = 5.83$ GHz	Surface 1: AMC #1	$\|\rho\|_{\text{AMC \#1}} = -6.3\,\text{dB}$ $<\rho>_{\text{AMC \#1}} = -75°$
	Surface 2: AMC #2	$\|\rho\|_{\text{AMC \#2}} = -6.3\,\text{dB}$ $<\rho>_{\text{AMC \#2}} = 66°$
	Reflection coefficient difference	$\|\rho\|_{\text{AMC \#1}} - \|\rho\|_{\text{AMC \#2}} = 0\,\text{dB}$ $<\rho>_{\text{AMC \#1}}$ $- <\rho>_{\text{AMC \#2}} = 141°$
Prototype AMC #1,3 RCS reduction: 11 dB @ $f = 6.15$ GHz	Surface 1: AMC #1	$\|\rho_{\text{AMC \#1}} = -0.1\,\text{dB}$ $<\rho>_{\text{AMC \#1}} = -165°$
	Surface 2: AMC #3	$\|\rho\|_{\text{AMC \#3}} = -5.8\,\text{dB}$ $<\rho>_{\text{AMC \#3}} = -79°$
	Reflection coefficient difference	$\|\rho\|_{\text{AMC \#1}} - \|\rho\|_{\text{AMC \#3}} = -5.7\,\text{dB}$ $<\rho>_{\text{AMC \#1}}$ $- <\rho>_{\text{AMC \#3}} = 85°$

Using Table 1 reflection coefficient values, the scattered field is computed for each combination of incidence and scattering angles: prototype surface is discretized in $0.05\lambda \times 0.05\lambda$ square patches, assigning the proper resulting reflection coefficient value to each patch. The incident field is a spherical wave whose origin is placed at the same relative position as the Tx horn antenna inside the anechoic chamber. The scattered field is evaluated at a point made coincident with the measurement positions inside the measurement facility.

Figure 6 compares the measured and simulated RCS for quasi-normal incidence for all the frequency range. Differences between simulations and measurements show that measured RCS is larger than the predicted from the Array Factor Theory using the measured values of reflection coefficient for manufactured prototypes, especially in the case of AMC #1,2, not only regarding the RCS value, but also, and even more remarkable, the RCS reduction bandwidth. Thus, the significant RCS reduction achieved when AMC operation bands overlap
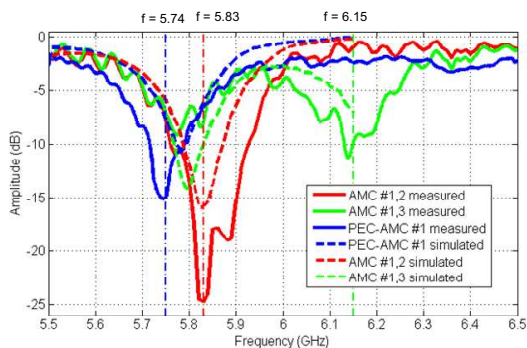
Figure 6. Comparison between simulated and measured scattered field amplitude for prototypes AMC #1,2, AMC #1,3 and AMC #1-PEC. Quasi-normal incidence ($\theta_{\mathrm{inc}} = \theta_{\mathrm{scatt}} = 2.3°$, $\varphi = 0°$).

could be better explained from coupling resonators phenomena, as the Array Factor Theory is not able to predict such significant RCS reduction.

3.4. Characterization Regarding Different Azimuth Angles (θ_{az})

RCS reduction effectiveness has been tested for different azimuth angles (θ_{az}), keeping the Tx and Rx horn antenna placement fixed. $f = 5.83$ is selected for the prototype AMC #1,2 (which is inside the frequency band where the RCS is reduced more than 15 dB, as depicted in Fig. 5). In the case of the AMC #1,3 and AMC #1-PEC, the selected frequencies are $f = 6.15$ GHz and $f = 5.74$ GHz respectively.

Figure 7 compares the normalized scattered field amplitude vs. θ_{az} angle of a metallic plate (black line) and the AMC #1,2 prototype (red line). The maximum of the measured metallic plate RCS for $\varphi = 0°$ (in the $\theta_{\mathrm{az}} = [-50°, +50°]$ interval) is about 12 dB higher than the maximum of the AMC #1,2 scattered field. However, for $\varphi = 45°$, the measured AMC #1,2 scattered field level maximum raises until -7 dB with respect to the maximum of the metallic plate because of a constructive interference depending on the θ_{az} angle, AMC electric size, and reflection coefficient of unit cells AMC #1 and AMC #2 [30, 31].

With respect to the AMC #1,3 (Fig. 7, green line), the RCS reduction is worse than AMC #1,2: a 12 dB decrease is obtained for $\theta_{\mathrm{az}} = 0°$, less than half of the AMC #1,2 prototype RCS reduction (25 dB, see Fig. 7).

It is possible to appreciate similarities between AMC #1,3 and AMC #1-PEC (Fig. 7, blue line), especially for $\varphi = 45°$. The
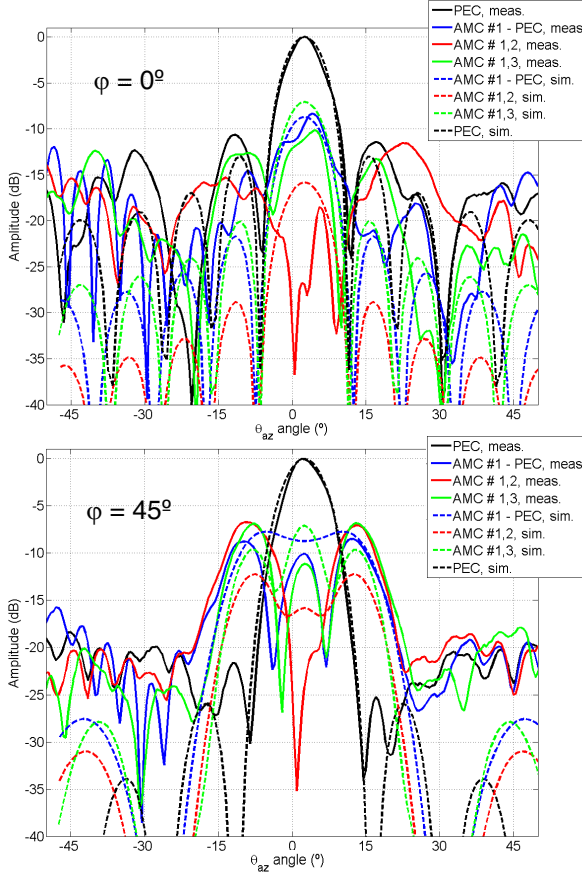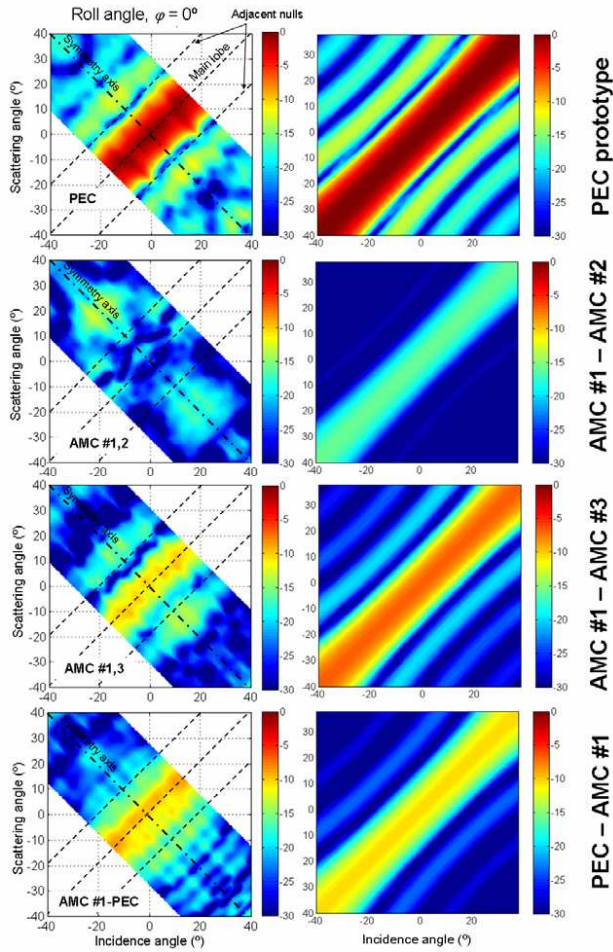
Figure 7. Normalized scattered field amplitude as a function of the θ_{az}. AMC #1,2 (frequency, $f = 5.83\,\text{GHz}$). AMC #1,3 (frequency, $f = 6.15\,\text{GHz}$). AMC #1-PEC (frequency, $f = 5.74\,\text{GHz}$). Comparison between measurements and simulations.

explanation is the following: in the case of AMC #1,3, when one of the two AMC surfaces has a 0° reflection phase, the other AMC surface reflection phase is close to the ±180° value (that is, a PEC behavior, see Fig. 2).

Measurement results plotted in Fig. 7 (with solid lines) have been compared with the simulated scattered fields using the Array Factor Theory (dashed lines). The metallic plate RCS is also plotted in order to have a reference result, showing a good agreement with measurements. It is noticed that the Array Factor Theory fails in predicting the null that the AMC #1,2 pattern has at $\theta_{\text{az}} = 0°$ for

both $\varphi = 0°$ and $\varphi = 45°$. For the rest of the cases, the agreement is acceptable although AMC #1-PEC nulls at $\theta_{\mathrm{az}} = \pm 5°$ for $\varphi = 45°$ are not predicted. It can be remarked that better agreement between simulation and measurements is observed for AMC #1,3 because the AMC operation bandwidths are not overlapped.

Figure 8. Scattered field (normalized amplitude, dB) as a function of the incidence angle (θ_{inc}) and the scattering angle (θ_{scatt}). Roll angle $\varphi = 0°$. Right column plots: simulation using Array Factor Theory. Left column plots: measured scattered field in anechoic chamber. Dashed lines represent the placement of the PEC scattered field main lobe and its adjacent nulls.

3.5. Characterization Regarding Different Incident and Scattering Angles

Next, the fields scattered by the metallic plate and the AMC prototypes have been evaluated for different incidence and scattering angles. The scattered field amplitude from the metallic plate, and from prototypes
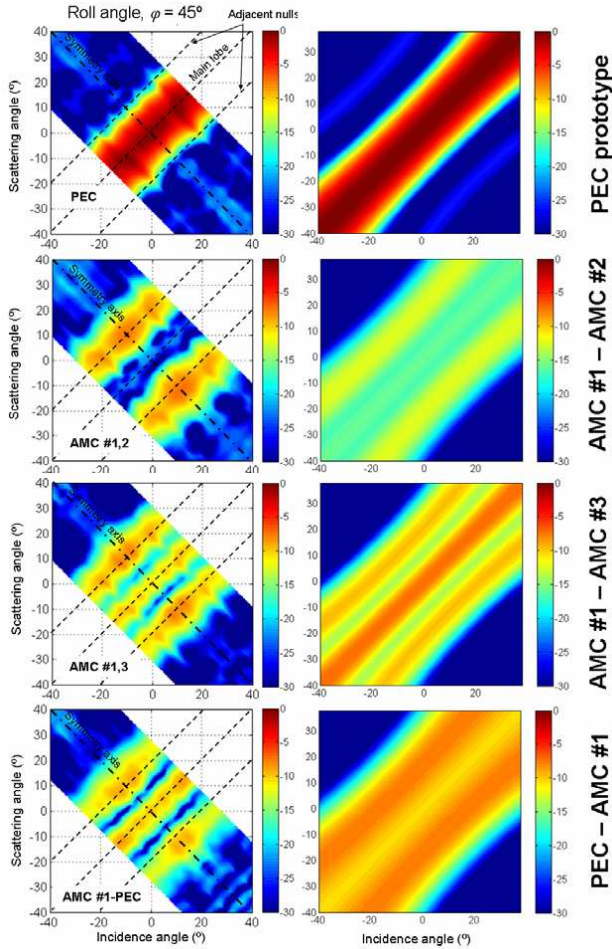
Figure 9. Scattered field (normalized amplitude, dB) as a function of the incidence angle (θ_{inc}) and the scattering angle (θ_{scatt}). Roll angle $\varphi = 45°$. Right column plots: simulation using Array Factor Theory. Left column plots: measured scattered field in anechoic chamber. Dashed lines represent the placement of the PEC scattered field main lobe and its adjacent nulls.

AMC #1,2 ($f = 5.83\,\mathrm{GHz}$), AMC #1,3 ($f = 6.15\,\mathrm{GHz}$), and AMC #1-PEC ($f = 5.74\,\mathrm{GHz}$) are compared in Fig. 8 for a roll angle of $\varphi = 0°$, and Fig. 9 for $\varphi = 45°$.

For those positions where $\theta_{\mathrm{inc}} = \theta_{\mathrm{scatt}}$ and $\varphi = 0°$ the field scattered by the AMC #1,2 is 20 dB below the metallic plate level; in the case of $\varphi = 45°$, the scattered field pattern present two lobes whose normalized level is $-7\,\mathrm{dB}$.

The other prototypes (AMC #1,3 and AMC #1-PEC) present a higher scattered field level for $\theta_{\mathrm{inc}} = \theta_{\mathrm{scatt}}$, that is $-10\,\mathrm{dB}$. Once again, similarities between AMC #1,3 and AMC #1-PEC can be clearly appreciated in Fig. 8, especially for $\varphi = 45°$, presenting both prototypes a three-beam pattern.

Once again, measurement results have been compared with the simulated scattered field using the Array Factor Theory. In order to have a reference result, the metallic plate RCS is calculated, showing a good agreement with measurements both for $\varphi = 0°$ (main lobe and adjacent lobes) and $\varphi = 45°$ (main lobe). Similar agreement for both φ-angles can be seen in the case of AMC #1-PEC and AMC #1,3, especially in terms of scattered field levels.

However, for AMC #1,2 prototype, some discrepancies exist between simulation and measurements both in scattered field pattern and relative field levels. These differences can be justified from the fact that the Array Factor Theory do not take into account the coupling phenomena that occur when AMC operation bandwidth overlap.

4. CONCLUSION

The combination of PEC-AMC or two AMC surfaces with 180°-phaseshift in their reflection coefficients, but different reflection coefficient amplitudes, do not ensure a full destructive interference in the reflected field as can be extracted from results rendered in Fig. 5–Fig. 9. However, AMC #1,2 reports the best RCS reduction performance, combining two AMC surfaces with similar reflection coefficient amplitudes in their AMC operation bandwidth which overlap, although a 180°-phaseshift is not completely achieved.

Regarding the prototype based on the combination of AMCs with non-overlapped frequency bands (AMC #1,3), it has similar behavior as the AMC #1-PEC prototype, with the advantage of having two frequency bands ($f_1 = 5.77\,\mathrm{GHz}$, $f_2 = 6.15\,\mathrm{GHz}$) where the RCS is reduced.

With regards to simulation results using Array Factor Theory, it is observed a better agreement for those cases in which the AMC operation bandwidth are not overlapped, being difficult to

predict scattered field relative level and patterns when the bands are overlapped. These discrepancies can be due to coupling resonances between combined AMCs and so are even more remarkable attending to RCS reduction bandwidth: each AMC behaves as a parallel LC resonant circuit. The fact of combining them in a chessboard-like structure provided that their AMC operation bandwidth overlap (having them a phaseshift less than 180° but similar reflection coefficient amplitude) is similar to the coupling of two oscillators, resulting in a broaden bandwidth and lower quality factor.

Finally, the attractiveness of the presented AMC combination for RCS reduction relies not only on its effectiveness, but also in the AMC characteristics itself: the absence of via holes and its low profile make it very attractive due to its simple fabrication and integration, and low cost.

ACKNOWLEDGMENT

REFERENCES

1. Lee, K.-C., C.-W. Huang, and M.-C. Fang, "Radar target recognition by projected features of frequency-diversity RCS," *Progress In Electromagnetics Research*, Vol. 81, 121–133, 2008.

2. Li, N.-J., C.-F. Hu, L.-X. Zhang, and J.-D. Xu, "Overview of RCS extrapolation techniques to aircraft targets," *Progress In Electromagnetics Research B*, Vol. 9, 249–262, 2008.

3. Wang, W.-T., S.-X. Gong, Y.-J. Zhang, F.-T. Zha, J. Ling, and T. Wan, "Low RCS dipole array synthesis based on MoM-PSO hybrid algorithm," *Progress In Electromagnetics Research*, Vol. 94, 119–132, 2009.

4. Li, X.-F., Y.-J. Xie, and R. Yang, "Bistatic RCS prediction for complex targets using modified current marching technique," *Progress In Electromagnetics Research*, Vol. 93, 13–28, 2009.

5. Bourlier, C., H. He, J. Chauveau, R. Hémon, and P. Pouliguen, "RCS of large bent waveguide ducts from a modal analysis combined with the kirchhoff approximation," *Progress In Electromagnetics Research*, Vol. 88, 1–38, 2008.

6. Kim, B.-C., K.-K. Park, and H.-T. Kim, "Efficient RCS prediction method using angular division algorithm," *Journal of Electromagnetic Waves and Applications*, Vol. 23, No. 1, 65–74, 2009.

7. Wang, W.-T., S.-X. Gong, X. Wang, H.-W. Yuan, J. Ling, and T.-T. Wan, "RCS reduction of array antenna by using bandstop FSS reflector," *Journal of Electromagnetic Waves and Applications*, Vol. 23, No. 11–12, 1505–1514, 2009.

8. Park, K.-K. and H.-T. Kim, "RCS prediction acceleration and reduction of table size for the angular division algorithm," *Journal of Electromagnetic Waves and Applications*, Vol. 23, No. 11–12, 1657–1664, 2009.

9. Pouliguen, P., R. Hémon, C. Bourlier, J.-F. Damiens, and J. Saillard, "Analytical formulae for radar cross section of flat plates in near field and normal incidence," *Progress In Electromagnetics Research B*, Vol. 9, 263–279, 2008.

10. Chen, H. T., G.-Q. Zhu, and S.-Y. He, "Using genetic algorithm to reduce the radar cross section of three-dimensional anisotropic impedance object," *Progress In Electromagnetics Research B*, Vol. 9, 231–248, 2008.

11. Chen, H.-Y., P. Zhou, L. Chen, and L. Deng, "Study on the properties of surface waves in coated RAM layers and monostatic Rcsr performances of the coated slab," *Progress In Electromagnetics Research M*, Vol. 11, 123–135, 2010.

12. Abdelaziz, A. A., "Improving the performance of an antenna array by using radar absorbing cover," *Progress In Electromagnetics Research Letters*, Vol. 1, 129–138, 2008.

13. Bondeson, A., Y. Yang, and P. Weinerfelt, "Shape optimization for radar cross sections by a gradient method," *International Journal for Numerical Methods in Engineering*, Vol. 61, No. 5, 687–715, 2004.

14. Lee, C., S. Lee, and R. Chou, "RCS reduction of a cylindrical cavity by dielectric coating," *1986 Antennas and Propagation Society International Symposium*, Vol. 24, 305–308, 1986.

15. Mosallaei, H. and Y. Rahmat-Samii, "RCS reduction in planar, cylindrical, and spherical structures by composite coatings using genetic algorithms," *1999 Antennas and Propagation Society International Symposium*, Vol. 1, 438–441, 1999.

16. Zainud-Deen, S. H., A. Z. Botros, and M. S. Ibrahim, "Scattering from bodies coated with metamaterial using FDFD method," *Progress In Electromagnetics Research B*, Vol. 2, 279–290, 2008.

17. Hady, L. K. and A. A. Kishk, "Electromagnetic scattering from conducting circular cylinder coated by meta-materials and loaded with helical strips under oblique incidence," *Progress In Electromagnetics Research B*, Vol. 3, 189–206, 2008.

18. Martini, E., S. Maci, and A. D. Yaghian, "Phase and group velocities in three-dimensional ideal cloaks," *3rd European Conference on Antennas and Propagation*, 3244–3248, 2009.

19. Schurig, D., J. J. Mock, B. J. Justice, S. A. Cummer, J. B. Pendry, A. F. Starr, and D. R. Smith, "Metamaterial electromagnetic cloak at microwave frequencies," *Science*, Vol. 314, No. 5801, 977–980, 2006.

20. Salisbury, W. W., *Absorbent Body for Electromagnetic Waves*, US Patent 2 599 944, Jun. 10, 1952.

21. Fante, R. L. and M. T. McCormack, "Reflection properties of the Salisbury screen," *IEEE Transactions on Antennas and Propagation*, Vol. 36, No. 10, 1443–1454, Oct. 1988.

22. Abdelaziz, A. A., "A novel technique for improving the performance of Salisbury screen," *Progress In Electromagnetics Research Letters*, Vol. 1, 1–8, 2008.

23. Engheta, N., "Thin absorbing screens using metamaterial surfaces," *Proc. IEEE Antennas and Propagation Society International Symposium*, 392–395, 2002.

24. Oraizi, H. and A. Abdolali, "Combination of MLS, GA and CG for the reduction of RCS of multilayered cylindrical structures composed of dispersive metamaterials," *Progress In Electromagnetics Research B*, Vol. 3, 227–253, 2008.

25. Manapati, M. B. and R. S. Kshetrimayum, "SAR reduction in human head from mobile phone radiation using single negative metamaterials," *Journal of Electromagnetic Waves and Applications*, Vol. 23, No. 10, 1385–1395, 2009.

26. Li, M., H.-L. Yang, X.-W. Hou, Y. Tian, and D.-Y. Hou, "Perfect metamaterial absorber with dual bands," *Progress In Electromagnetics Research*, Vol. 108, 37–49, 2010.

27. Bucinskas, J., L. Nickelson, and V. Shugurovas, "Microwave scattering and absorption by a multilayered lossy metamaterial-glass cylinder," *Progress In Electromagnetics Research*, Vol. 105, 103–118, 2010.

28. Costa, F., A. Monorchio, and G. Manara, "Analysis and design of ultra thin electromagnetic absorbers comprising resistively loaded high impedance surfaces," *IEEE Transactions on Antennas and Propagation*, Vol. 58, No. 5, 1551–1558, May 2010.

29. Zhang, Y., R. Mittra, and B. Z. Wang, "Novel design for low-RCS screens using a combination of dual-AMC," *Antennas and Propagation Society Intl. Symposium, 2009, APSURSI '09*, 1–4, Jun. 1–5, 2009.

30. Paquay, M., J. C. Iriarte, I. Ederra, R. Gonzalo, and P. de Maagt, "Thin AMC structure for radar cross section reduction," *IEEE Transactions on Antennas and Propagation*, Vol. 55, No. 12, 3630–3638, Dec. 2007.

31. Iriarte, J. C., M. Paquay, I. Ederra, R. Gonzalo, and P. de Maagt, "RCS reduction in a chessboard-like structure using AMC cells," *2nd European Conference on Antennas and Propagation (EuCAP 2007)*, 1–4, Nov. 11–16, 2007.

32. Iriarte, J. C., I. Ederra, R. Gonzalo, and P. de Maagt, "Dual band RCS reduction using planar technology by combining AMC structures," *3rd European Conference on Antennas and Propagation (EuCAP 2009)*, 3708–3709, 2009.

33. Zhang, Y., R. Mittra, B. Z. Wang, and N. T. Huang, "AMCs for ultra-thin and broadband RAM design," *Electronics Letters*, Vol. 45, No. 10, 484–485, 2009.

34. Caloz, C., A. Sanada, and T. Itoh, "A novel composite right-/left-handed coupled-line directional coupler with arbitrary coupling level and broad bandwidth," *IEEE Transactions on Microwave Theory and Techniques*, Vol. 52, No. 3, 980–992, Mar. 2004.

35. De Cos, M. E., Y. Álvarez, and F. Las-Heras, "Planar artificial magnetic conductor: Design and characterization setup in the RFID SHF band," *Journal of Electromagnetic Waves and Applications*, Vol. 23, No. 11–12, 1467–1478, 2009.

36. Li, Y., et al., "Prototyping dual-band artificial magnetic conductors with laser micromachining," *Proc. of WARS2006 Conference*, Leura, NSW, Australia, Feb. 2006.

37. Alvarez, Y., M. E. De Cos, and F. Las-Heras, "RCS measurement setup for periodic structure prototype characterization," *IEEE Antennas and Propagation Magazine*, Vol. 52, No. 3, 100–106, Jun. 2010.

38. De Cos, M. E., Y. Álvarez Lopez, and F. Las-Heras, "A novel approach for RCS reduction using a combination of artificial magnetic conductors," *Progress In Electromagnetics Research*, Vol. 107, 147–159, 2010.